

Surface Integral Method for the Second Harmonic Generation in Metal Nanoparticles

Carlo Forestiere,^{1,2} Antonio Capretti,¹ and Giovanni Miano^{1,*}

¹*Department of Electrical Engineering and Information Technology,
Università degli Studi di Napoli Federico II, via Claudio 21, Napoli, 80125, Italy*

²*Department of Electrical and Computer Engineering & Photonics Center,
Boston University, 8 Saint Marys Street, Boston, Massachusetts*

Second harmonic (SH) radiation in metal nanoparticles is generated by both nonlocal-bulk and local-surface SH sources, induced by the electromagnetic field at the fundamental frequency. We propose a surface integral equation (SIE) method for evaluating the SH radiation generated by metal nanoparticles with arbitrary shapes, considering both the local-surface and nonlocal-bulk SH sources. We demonstrate that the contribution of the nonlocal-bulk SH source to the SH electromagnetic field can be rigorously taken into account through an equivalent surface magnetic current. We numerically solve the SIE problem by using the Galerkin method and the Rao-Wilton-Glisson basis functions in the framework of the distribution theory. The accuracy of the proposed method is verified by comparison with the SH-Mie formulation in the case of SH generation from a spherical nanoparticle. As an example of a complex-shaped particle, we investigate the SH radiation generated from a triangular nano-prism. The method paves the way for a better understanding of the SH generation process in arbitrarily shaped nanoparticles and can also have a high impact in the design of novel nanoplasmonic devices with enhanced SH emission.

I. INTRODUCTION

The study of nonlinear optical properties of noble metal nanoparticles (NPs) has become a very active research field, stimulated by both the maturity of nanofabrication techniques and the appeal of the potential applications. Noble metal nanoparticles support localized surface plasmon (LSP) resonances, consisting in the collective oscillations of the conduction electrons [1]. LSPs can significantly enhance both the linear and nonlinear scattering processes [2], enabling strong nonlinear optical processes at relatively low excitation powers.

The second harmonic (SH) generation is a nonlinear optical process in which two photons of the same frequency, *i.e.* the fundamental frequency, interact with the material and generate one photon of twice the frequency. SH generation from noble metal NPs takes place in the bulk of the particle and on its surface. In particular, the electromagnetic field at the fundamental frequency induces nonlocal-bulk and local-surface SH sources, whereas the local-bulk SH source is absent due to the centrosymmetry of the material [3]. The local-surface SH source is due to the symmetry breaking at the interface between the NP and the embedding medium [4]. The relative contribution to the SH radiation of nonlocal-bulk and local-surface sources depend on the NP shape and size, and on the optical properties of the metal at both the fundamental and the SH frequencies [5].

Several analytical models have been developed to describe the SHG from noble metals NPs of simple shapes such as spheres and cylinders. In particular, Dadap *et al.* [4] studied the SH radiation generated from the local-surface SH source in a sphere with radius much smaller

than the wavelength of the exciting light (Rayleigh limit). This model was later extended in [6, 7], considering also the nonlocal-bulk source. A full-wave theory of the SH generation by a sphere of centrosymmetric material featuring SH local-surface sources has been proposed in [8]. This approach has been recently extended to model aggregates of spheres [9] but, also in this case, only the local-surface SH sources have been taken into account. A full-wave analytical theory has been also proposed for the SH scattering of light by a cylinder of infinite length [10].

The last few decades have witnessed a continuous improvement of nanofabrication techniques and a large variety of complex shapes can be controllably achieved nowadays. This fact allows for an accurate tuning of the spectral position of the LSP resonance of a NP and stimulates the demand for numerical tools to model the linear [11] and non-linear behavior of NPs with arbitrary shapes. In fact, De Beer *et al.* [12] presented a theoretical framework for solving the SH generation problem for particles with arbitrary shapes in the low contrast limit. Makitalo *et al.* [13] introduced a surface integral equation (SIE) formulation for studying the nonlinear scattering from arbitrarily shaped particles taking into account only the local-surface SH sources. However, the validity of their numerical formulation will be questioned in the present paper. Benedetti *et al.* [14] developed a volume integral equation (VIE) formulation based on the dyadic Green function for the study of non-linear scattering properties from arbitrarily shaped particles due to both nonlocal-bulk and local-surface contributions. However, unlike SIE formulations, the VIE formulations require the discretization of the entire NP volume, resulting in an higher memory occupancy and longer computational time.

In this paper, we present a SIE formulation of the SH generation problem for three dimensional, arbitrarily shaped nanoparticles made of centrosymmetric and

* Corresponding author: miano@unina.it

lossy materials, that accounts for both the nonlocal-bulk and local-surface nonlinear polarization sources. The problem is treated in the frequency domain under the undepleted-pump approximation. In particular, we demonstrate that the contribution of the nonlocal-bulk source to the SH electromagnetic field can be taken into account by introducing an equivalent surface magnetic current on the particle boundary, leading to a great simplification of the numerical problem. Unlike ref. [13], the numerical formulation has been derived in the framework of the distribution theory in order to correctly account for the discontinuity of the discrete representation of the SH sources.

The paper is organized as follows. Section 2 presents the mathematical statement of the problem along with the expression of both the nonlocal-bulk and the local-surface nonlinear polarization sources of the SH radiation. Then Section 3 is devoted to the SIE formulation and its numerical solution through the Galerkin method. Section 4 deals with the validation of the method, accomplished through an extensive comparison with the full wave SHG Mie theory for nanoparticles with spherical shapes proposed in ref. [15]. Finally, the SHG for a gold triangular prism is presented.

II. STATEMENT OF THE PROBLEM

In this section, we formulate the problem of SH generation from a lossy NP of arbitrary shape in a homogeneous medium, when it is illuminated by a time-harmonic electromagnetic field at frequency ω . The domain of the electromagnetic field is the entire space \mathbb{R}^3 , which is divided into the interior of the metal domain $\overset{\circ}{V}_i$, the external medium $\overset{\circ}{V}_e$ and the interface S . The closed surface S is oriented such that its normal \mathbf{n} points outward. Furthermore, \mathbf{r} denotes the position vector with respect to an arbitrary reference point O . Since the intensities of the SH fields generated by noble metals NP are always order of magnitude weaker than the intensities of the pump fields, we can assume that the SH fields do not couple back to the fundamental fields (*undepleted-pump approximation*). Therefore, the non-linear electromagnetic problem can be decomposed in two linear scattering problems at the fundamental frequency and at the SH frequency, and the nonlinear response of the material is phenomenologically described by SH polarization sources induced by the fundamental electric field.

We denote with $(\mathbf{E}_l^{(\omega)}, \mathbf{H}_l^{(\omega)})$ the fundamental fields at frequency ω in the region $\overset{\circ}{V}_l$ with $l = i, e$, and with $(\mathbf{E}_l^{(2\omega)}, \mathbf{H}_l^{(2\omega)})$ the SH field at frequency 2ω . We use the convention $\mathbf{a}(\mathbf{r}) = \Re\{\mathbf{A}^{(\Omega)}(\mathbf{r}) \exp(j\Omega t)\}$ for representing a time harmonic electromagnetic field. Furthermore, we denote with $(\mathbf{E}_0^{(\omega)}, \mathbf{H}_0^{(\omega)})$ the pump fields incident in $\overset{\circ}{V}_e$, with $(\varepsilon_i\{\Omega\}, \mu_i)$ the linear permittivity at frequency

Ω and the permeability of the metal and with and (ε_e, μ_e) the permeability and the permittivity of the embedding medium. In order to calculate the SH radiation generated by the metal particle we have to evaluate: 1) the electric fields $\mathbf{E}_l^{(\omega)}$ at the fundamental frequency induced by the pump electromagnetic field; 2) the bulk and surface nonlinear sources generated by $\mathbf{E}_l^{(\omega)}$ and 3) the SH fields $(\mathbf{E}_l^{(2\omega)}, \mathbf{H}_l^{(2\omega)})$ generated by the nonlinear sources.

Aiming at the solution of scattering problem at the fundamental frequency, we introduce the scattered fields $(\mathbf{E}_l^{(\omega,s)}, \mathbf{H}_l^{(\omega,s)})$ with $l = i, e$, defined as:

$$\begin{cases} \mathbf{E}_e^{(\omega,s)} = \mathbf{E}_e^{(\omega)} - \mathbf{E}_0^{(\omega)} \\ \mathbf{H}_e^{(\omega,s)} = \mathbf{H}_e^{(\omega)} - \mathbf{H}_0^{(\omega)} \end{cases} \text{ in } \overset{\circ}{V}_e \quad \begin{cases} \mathbf{E}_i^{(\omega,s)} = \mathbf{E}_i^{(\omega)} \\ \mathbf{H}_i^{(\omega,s)} = \mathbf{H}_i^{(\omega)} \end{cases} \text{ in } \overset{\circ}{V}_i \quad (1)$$

The scattered fields at the fundamental frequency can be determined by solving the problem:

$$\begin{cases} \nabla \times \mathbf{E}_l^{(\omega,s)} = -j\omega\mu_l \mathbf{H}_l^{(\omega,s)} \\ \nabla \times \mathbf{H}_l^{(\omega,s)} = j\omega\varepsilon_l\{\omega\} \mathbf{E}_l^{(\omega,s)} \end{cases} \text{ in } \overset{\circ}{V}_l, \quad \text{with } l = i, e, \\ \begin{cases} \mathbf{n} \times (\mathbf{E}_e^{(\omega,s)} - \mathbf{E}_i^{(\omega,s)}) = -\mathbf{n} \times \mathbf{E}_0^{(\omega)} \\ \mathbf{n} \times (\mathbf{H}_e^{(\omega,s)} - \mathbf{H}_i^{(\omega,s)}) = -\mathbf{n} \times \mathbf{H}_0^{(\omega)} \end{cases} \text{ on } S, \end{cases} \quad (2)$$

with the radiation condition at infinity.

Once the solution of problem 2 has been obtained, the SH polarization sources can be calculated. Noble metals are centrosymmetric materials, therefore the leading term of the bulk nonlinear polarization density $\mathbf{P}_b^{(2\omega)}$ is:

$$\mathbf{P}_b^{(2\omega)} = \varepsilon_0 \overset{\leftrightarrow}{\chi}_b^{(2)} : \mathbf{E}_i^{(\omega)} (\nabla \mathbf{E}_i^{(\omega)}) \quad \text{for } \mathbf{r} \in \overset{\circ}{V}_i \quad (3)$$

where $\overset{\leftrightarrow}{\chi}_b^{(2)}$ is the quadrupolar contribution to the second-order nonlinear bulk susceptibility of the metal. Noble metals also are isotropic, in the case of homogeneous material the relation 3 becomes

$$\mathbf{P}_b^{(2\omega)} = \varepsilon_0 \gamma^{(2)} \nabla (\mathbf{E}_i^{(\omega)} \cdot \mathbf{E}_i^{(\omega)}) + \varepsilon_0 \delta^{(2)} (\mathbf{E}_i^{(\omega)} \cdot \nabla) \mathbf{E}_i^{(\omega)}, \quad (4)$$

where $\gamma^{(2)}$ and $\delta^{(2)}$ are material parameters. Measurements indicate that the second term in 4 is negligible with respect to the second one [16]. Therefore, the bulk polarization source is:

$$\mathbf{P}_b^{(2\omega)} = \varepsilon_0 \gamma^{(2)} \nabla (\mathbf{E}_i^{(\omega)} \cdot \mathbf{E}_i^{(\omega)}). \quad (5)$$

The local-surface SH polarization source $\mathbf{P}_S^{(2\omega)}$ is:

$$\mathbf{P}_S^{(2\omega)} = \varepsilon_0 \overset{\leftrightarrow}{\chi}_S^{(2)} : \mathbf{E}_i^{(\omega)} \mathbf{E}_i^{(\omega)}, \quad (6)$$

where $\overset{\leftrightarrow}{\chi}_S^{(2)}$ is the second-order surface nonlinear susceptibility. Since the nanoparticle surface has an isotropic

symmetry with a mirror plane perpendicular to it, the surface-susceptibility tensor $\overset{\leftrightarrow}{\chi}_S^{(2)}$ has only three non-vanishing and independent elements, $\chi_{\perp\perp\perp}^{(2)}$, $\chi_{\perp\parallel\parallel}^{(2)}$ and $\chi_{\parallel\perp\perp}^{(2)} = \chi_{\parallel\parallel\perp}^{(2)}$, where \perp and \parallel refer to the orthogonal and tangential components to the nanoparticle surface. Therefore, we have:

$$\mathbf{P}_S^{(2\omega)} = \epsilon_0 \left[\chi_{\perp\perp\perp}^{(2)} \mathbf{nnn} + \chi_{\perp\parallel\parallel}^{(2)} (\mathbf{nt}_1\mathbf{t}_1 + \mathbf{nt}_2\mathbf{t}_2) + \chi_{\parallel\perp\perp}^{(2)} (\mathbf{t}_1\mathbf{nt}_1 + \mathbf{t}_2\mathbf{nt}_2) \right] : \mathbf{E}_i^{(\omega)} \mathbf{E}_i^{(\omega)}, \quad (7)$$

where $(\mathbf{t}_1, \mathbf{t}_2, \mathbf{n})$ is a system of three orthonormal vectors locally defined on the particle surface. The contribution of tangential and normal component of the surface nonlinear polarization are taken into account by introducing the surface electric $\boldsymbol{\pi}_e^{(2\omega)}$ and magnetic $\boldsymbol{\pi}_m^{(2\omega)}$ current density :

$$\boldsymbol{\pi}_e^{(2\omega)} = j2\omega \mathbf{P}_{S,t}^{(2\omega)}, \quad (8a)$$

$$\boldsymbol{\pi}_m^{(2\omega)} = \frac{1}{\epsilon_0} \mathbf{n} \times \nabla_S P_{S,n}^{(2\omega)}, \quad (8b)$$

where $\mathbf{P}_{S,t}^{(2\omega)} = -\mathbf{n} \times \mathbf{n} \times \mathbf{P}_S^{(2\omega)}$ and $P_{S,n}^{(2\omega)} = \mathbf{P}_S^{(2\omega)} \cdot \mathbf{n}$.

Once the phenomenological sources are known, we can determine the SH fields by solving non-homogeneous problem:

$$\begin{cases} \nabla \times \mathbf{E}_e^{(2\omega)} = -j2\omega\mu_e \mathbf{H}_e^{(2\omega)} \\ \nabla \times \mathbf{H}_e^{(2\omega)} = j2\omega\epsilon_e \mathbf{E}_e^{(2\omega)} \end{cases} \text{ in } \overset{\circ}{V}_e, \quad (9a)$$

$$\begin{cases} \nabla \times \mathbf{E}_i^{(2\omega)} = -j2\omega\mu_i \mathbf{H}_i^{(2\omega)} \\ \nabla \times \mathbf{H}_i^{(2\omega)} = j2\omega\epsilon_i \{2\omega\} \mathbf{E}_i^{(2\omega)} + j2\omega P_b \end{cases} \text{ in } \overset{\circ}{V}_i, \quad (9b)$$

$$\begin{cases} \mathbf{n} \times (\mathbf{E}_e^{(2\omega)} - \mathbf{E}_i^{(2\omega)}) = -\boldsymbol{\pi}_m^{(2\omega)} \\ \mathbf{n} \times (\mathbf{H}_e^{(2\omega)} - \mathbf{H}_i^{(2\omega)}) = \boldsymbol{\pi}_e^{(2\omega)} \end{cases} \text{ on } S, \quad (9c)$$

with the radiation condition at infinity. Due to the linearity of the problem 9a-9c, its general solution is the sum of the solution of the homogeneous equation and one particular solution of the inhomogeneous equation. The equations 9a and 9b are satisfied by a vanishing magnetic field and by the electric field:

$$\mathbf{E}_{part}^{(2\omega)} = \begin{cases} \mathbf{0} & \text{if } \mathbf{r} \in \overset{\circ}{V}_e, \\ -\frac{\epsilon_0\gamma^{(2)}}{\epsilon_i\{2\omega\}} \nabla (\mathbf{E}_i^{(\omega)} \cdot \mathbf{E}_i^{(\omega)}) & \text{if } \mathbf{r} \in \overset{\circ}{V}_i. \end{cases} \quad (10)$$

Therefore, the solution of the non-homogeneous problem defined by eqs. 9a-9c can be written as:

$$\begin{cases} \mathbf{E}_l^{(2\omega)} = \tilde{\mathbf{E}}_l^{(2\omega)} + \mathbf{E}_{part}^{(2\omega)} \\ \mathbf{H}_l^{(2\omega)} = \tilde{\mathbf{H}}_l^{(2\omega)} \end{cases} \text{ with } l = i, e, \quad (11)$$

where $(\tilde{\mathbf{E}}_l^{(2\omega)}, \tilde{\mathbf{H}}_l^{(2\omega)})$ with $l = i, e$ is the solution of the

problem:

$$\begin{cases} \nabla \times \tilde{\mathbf{E}}_l^{(2\omega)} = -j2\omega\mu_l \tilde{\mathbf{H}}_l^{(2\omega)} \\ \nabla \times \tilde{\mathbf{H}}_l^{(2\omega)} = j2\omega\epsilon_l \{2\omega\} \tilde{\mathbf{E}}_l^{(2\omega)} \end{cases} \text{ in } \overset{\circ}{V}_l \text{ with } l = i, e, \\ \begin{cases} \mathbf{n} \times (\tilde{\mathbf{E}}_e^{(2\omega)} - \tilde{\mathbf{E}}_i^{(2\omega)}) = -\boldsymbol{\pi}_m^{(2\omega)} - \boldsymbol{\pi}_b^{(2\omega)} \\ \mathbf{n} \times (\tilde{\mathbf{H}}_e^{(2\omega)} - \tilde{\mathbf{H}}_i^{(2\omega)}) = \boldsymbol{\pi}_e^{(2\omega)} \end{cases} \text{ on } S, \end{cases} \quad (12)$$

with the radiation condition at infinity, where:

$$\boldsymbol{\pi}_b^{(2\omega)} = \frac{1}{\epsilon_0} \mathbf{n} \times \nabla_S P_{b,n}^{(2\omega)}, \quad (13)$$

and

$$P_{b,n}^{(2\omega)} = \frac{\epsilon_0^2 \gamma^{(2)}}{\epsilon_i \{2\omega\}} (\mathbf{E}_i^{(\omega)} \cdot \mathbf{E}_i^{(\omega)}). \quad (14)$$

In conclusion, the nonlocal bulk source can be equivalently treated by using a superficial magnetic current, associated to a fictitious surface polarization $P_{b,n}^{(2\omega)} \mathbf{n}$.

III. SURFACE INTEGRAL EQUATIONS

Let us define, for the same geometry described in the previous section, an auxiliary scattering problem that includes both the fundamental and the SH problems as special cases. Let $\boldsymbol{\pi}_0^{(\Omega,e)}$, $\boldsymbol{\pi}_0^{(\Omega,m)}$ be the impressed electric and magnetic sources on S . We denote with $(\mathbf{E}_l^{(\Omega,s)}, \mathbf{H}_l^{(\Omega,s)})$ $l = i, e$ the fields solution of the problem:

$$\begin{cases} \nabla \times \mathbf{E}_l^{(\Omega,s)} = -j\Omega\mu_l \mathbf{H}_l^{(\Omega,s)} \\ \nabla \times \mathbf{H}_l^{(\Omega,s)} = j\Omega\epsilon_l \{\Omega\} \mathbf{E}_l^{(\Omega,s)} \end{cases} \text{ in } \overset{\circ}{V}_l \text{ with } l = i, e, \\ \begin{cases} \mathbf{n} \times (\mathbf{E}_e^{(\Omega,s)} - \mathbf{E}_i^{(\Omega,s)}) = -\boldsymbol{\pi}_0^{(\Omega,m)} \\ \mathbf{n} \times (\mathbf{H}_e^{(\Omega,s)} - \mathbf{H}_i^{(\Omega,s)}) = +\boldsymbol{\pi}_0^{(\Omega,e)} \end{cases} \text{ on } S, \end{cases} \quad (15)$$

with the radiation condition at infinity. We obtain the fundamental problem described of eq. 2, by substituting $\Omega = \omega$ and

$$\begin{cases} \boldsymbol{\pi}_0^{(\omega,e)} = -\mathbf{n} \times \mathbf{H}_0^{(\omega)}, \\ \boldsymbol{\pi}_0^{(\omega,m)} = \mathbf{n} \times \mathbf{E}_0^{(\omega)}. \end{cases} \quad (16)$$

Analogously, we can obtain the SH problem described by eq. 12 by substituting $\Omega = 2\omega$ and

$$\begin{cases} \boldsymbol{\pi}_0^{(2\omega,e)} = \boldsymbol{\pi}_e^{(2\omega)}, \\ \boldsymbol{\pi}_0^{(2\omega,m)} = \boldsymbol{\pi}_m^{(2\omega)} + \boldsymbol{\pi}_b^{(2\omega)}. \end{cases} \quad (17)$$

We now derive the surface integral formulation for the problem of eq. 15. By invoking the Love's equivalent principle [17] for the exterior medium, the region $\overset{\circ}{V}_i$

is filled up with the same material of the region $\overset{\circ}{V}_e$, and the sources are removed. The equivalent currents $(\mathbf{j}_e^{(\Omega,e)}, \mathbf{j}_e^{(\Omega,m)})$, positioned on the external page S_e of the surface S , produce the field $(\mathbf{E}_e^{(\Omega,s)}, \mathbf{H}_e^{(\Omega,s)})$ in the region $\overset{\circ}{V}_e$, and null fields in the region $\overset{\circ}{V}_i$, *i.e.*:

$$\begin{aligned} \mathcal{E}_e^{(\Omega)} \{ \mathbf{j}_e^{(\Omega,e)}, \mathbf{j}_e^{(\Omega,m)} \} (\mathbf{r}) &= \begin{cases} \mathbf{0} & \text{if } \mathbf{r} \in \overset{\circ}{V}_i, \\ \mathbf{E}_e^{(\Omega,s)}(\mathbf{r}) & \text{if } \mathbf{r} \in \overset{\circ}{V}_e, \end{cases} \\ \mathcal{H}_e^{(\Omega)} \{ \mathbf{j}_e^{(\Omega,e)}, \mathbf{j}_e^{(\Omega,m)} \} (\mathbf{r}) &= \begin{cases} \mathbf{0} & \text{if } \mathbf{r} \in \overset{\circ}{V}_i, \\ \mathbf{H}_e^{(\Omega,s)}(\mathbf{r}) & \text{if } \mathbf{r} \in \overset{\circ}{V}_e, \end{cases} \end{aligned} \quad (18)$$

where the sources $(\mathbf{j}_e^{(\Omega,e)}, \mathbf{j}_e^{(\Omega,m)})$ are given by:

$$\begin{cases} \mathbf{j}_e^{(\Omega,e)} = + \mathbf{n} \times \mathbf{H}_e^{(\Omega,s)} \Big|_{S_e}, \\ \mathbf{j}_e^{(\Omega,m)} = - \mathbf{n} \times \mathbf{E}_e^{(\Omega,s)} \Big|_{S_e}. \end{cases} \quad (19)$$

An equivalent problem may be set up also for the region $\overset{\circ}{V}_i$. In this case the region $\overset{\circ}{V}_i$ is filled up with the material with electromagnetic parameters $(\varepsilon_i \{ \Omega \}, \mu_i)$. The equivalent currents $(\mathbf{j}_i^{(\Omega,e)}, \mathbf{j}_i^{(\Omega,m)})$, defined on the internal page S_i of the surface S , produce the original fields in the region $\overset{\circ}{V}_i$ and null field in the region $\overset{\circ}{V}_e$, *i.e.*

$$\begin{aligned} \mathcal{E}_i^{(\Omega)} \{ \mathbf{j}_i^{(\Omega,e)}, \mathbf{j}_i^{(\Omega,m)} \} (\mathbf{r}) &= \begin{cases} \mathbf{E}_i^{(\Omega,s)}(\mathbf{r}) & \text{if } \mathbf{r} \in \overset{\circ}{V}_i, \\ \mathbf{0} & \text{if } \mathbf{r} \in \overset{\circ}{V}_e, \end{cases} \\ \mathcal{H}_i^{(\Omega)} \{ \mathbf{j}_i^{(\Omega,e)}, \mathbf{j}_i^{(\Omega,m)} \} (\mathbf{r}) &= \begin{cases} \mathbf{H}_i^{(\Omega,s)}(\mathbf{r}) & \text{if } \mathbf{r} \in \overset{\circ}{V}_i, \\ \mathbf{0} & \text{if } \mathbf{r} \in \overset{\circ}{V}_e, \end{cases} \end{aligned} \quad (20)$$

where the sources $(\mathbf{j}_i^{(\Omega,e)}, \mathbf{j}_i^{(\Omega,m)})$ are given by:

$$\begin{cases} \mathbf{j}_i^{(\Omega,e)} = - \mathbf{n} \times \mathbf{H}_i^{(\Omega,s)} \Big|_{S_i}, \\ \mathbf{j}_i^{(\Omega,m)} = + \mathbf{n} \times \mathbf{E}_i^{(\Omega,s)} \Big|_{S_i}. \end{cases} \quad (21)$$

Furthermore, the sets of equivalent currents $(\mathbf{j}_e^{(\Omega,e)}, \mathbf{j}_e^{(\Omega,m)})$ and $(\mathbf{j}_i^{(\Omega,e)}, \mathbf{j}_i^{(\Omega,m)})$ are not independent. In fact, combining the boundary conditions of the problem 15 and the definitions 19 and 21 we obtain:

$$\begin{cases} \mathbf{j}_i^{(\Omega,e)} + \mathbf{j}_e^{(\Omega,e)} = \boldsymbol{\pi}_0^{(\Omega,e)}, \\ \mathbf{j}_i^{(\Omega,m)} + \mathbf{j}_e^{(\Omega,m)} = \boldsymbol{\pi}_0^{(\Omega,m)}. \end{cases} \quad (22)$$

We now consider the limit of eqs. 18 and 20 as the point \mathbf{r} approaches the surface S from its external face S_e and internal face S_i . Projecting the resulting equations

on the surface S we obtain:

$$\left(\mathcal{E}_e^{(\Omega,t)} \{ \mathbf{j}_e^{(\Omega,e)}, \mathbf{j}_e^{(\Omega,m)} \} \right) \Big|_{S_e} - \mathbf{n} \times \mathbf{j}_e^{(\Omega,m)} = \mathbf{0}, \quad (23a)$$

$$\left(\mathcal{H}_e^{(\Omega,t)} \{ \mathbf{j}_e^{(\Omega,e)}, \mathbf{j}_e^{(\Omega,m)} \} \right) \Big|_{S_e} + \mathbf{n} \times \mathbf{j}_e^{(\Omega,e)} = \mathbf{0}, \quad (23b)$$

$$\left(\mathcal{E}_i^{(\Omega,t)} \{ \mathbf{j}_i^{(\Omega,e)}, \mathbf{j}_i^{(\Omega,m)} \} \right) \Big|_{S_i} + \mathbf{n} \times \mathbf{j}_i^{(\Omega,m)} = \mathbf{0}, \quad (23c)$$

$$\left(\mathcal{H}_i^{(\Omega,t)} \{ \mathbf{j}_i^{(\Omega,e)}, \mathbf{j}_i^{(\Omega,m)} \} \right) \Big|_{S_i} - \mathbf{n} \times \mathbf{j}_i^{(\Omega,e)} = \mathbf{0}, \quad (23d)$$

where we have defined the operators:

$$\begin{aligned} \mathcal{E}_l^{(\Omega,t)} \{ \mathbf{j}^{(e)}, \mathbf{j}^{(m)} \} &= - \mathbf{n} \times \mathbf{n} \times \mathcal{E}_l^{(\Omega)} \{ \mathbf{j}^{(e)}, \mathbf{j}^{(m)} \} \Big|_{S_l}, \\ \mathcal{H}_l^{(\Omega,t)} \{ \mathbf{j}^{(e)}, \mathbf{j}^{(m)} \} &= - \mathbf{n} \times \mathbf{n} \times \mathcal{H}_l^{(\Omega)} \{ \mathbf{j}^{(e)}, \mathbf{j}^{(m)} \} \Big|_{S_l}. \end{aligned} \quad (24)$$

Eqs. 23a, 23c are the *T-electric field integral equations* (T-EFIE), eqs. 23d, 23b are the *T-magnetic field integral equations* (T-MFIE). By subtracting eq. 23c from eq. 23a and eq. 23d from 23b and substituting the expressions of the operators $\mathcal{E}_l^{(\Omega)}$, $\mathcal{H}_l^{(\Omega)}$, provided in the appendix A, we obtain the PMCHWT formulation:

$$\mathcal{C}^{(\Omega)} \mathbf{x}^{(\Omega)} = \mathbf{y}^{(\Omega)}, \quad (25)$$

where we have defined the operator $\mathcal{C}^{(\Omega)}$

$$\mathcal{C}^{(\Omega)} = \begin{vmatrix} \zeta_e \mathcal{T}_e^{(\Omega,t)} & + \mathcal{K}_e^{(\Omega,t)} & - \zeta_i \mathcal{T}_i^{(\Omega,t)} & - \mathcal{K}_i^{(\Omega,t)} \\ - \mathcal{K}_e^{(\Omega,t)} & \zeta_e^{-1} \mathcal{T}_e^{(\Omega,t)} & + \mathcal{K}_i^{(\Omega,t)} & - \zeta_i^{-1} \mathcal{T}_i^{(\Omega,t)} \\ \mathcal{I} & \mathbf{0} & \mathcal{I} & \mathbf{0} \\ \mathbf{0} & \mathcal{I} & \mathbf{0} & \mathcal{I} \end{vmatrix}, \quad (26)$$

the vector of unknowns $\mathbf{x}^{(\Omega)}$, and the excitation vector $\mathbf{y}^{(\Omega)}$

$$\mathbf{x}^{(\Omega)} = \begin{vmatrix} \mathbf{j}_e^{(\Omega,e)} \\ \mathbf{j}_e^{(\Omega,m)} \\ \mathbf{j}_i^{(\Omega,e)} \\ \mathbf{j}_i^{(\Omega,m)} \end{vmatrix}, \quad \mathbf{y}^{(\Omega)} = \begin{vmatrix} \frac{1}{2} \mathbf{n} \times \boldsymbol{\pi}_0^{(\Omega,m)} \\ - \frac{1}{2} \mathbf{n} \times \boldsymbol{\pi}_0^{(\Omega,e)} \\ \boldsymbol{\pi}_0^{(\Omega,e)} \\ \boldsymbol{\pi}_0^{(\Omega,m)} \end{vmatrix}, \quad (27)$$

and $\zeta_l \{ \Omega \} = \sqrt{\mu_l / \varepsilon_l} \{ \Omega \}$, with $l = i, e$. The expression of the operators $\mathcal{T}_l^{(\Omega,t)}$ and $\mathcal{K}_e^{(\Omega,t)}$ can be found in the appendix A. The expression of the excitation vector does not agree with the corresponding expression provided in [13].

IV. NUMERICAL SOLUTIONS

In the present section, we describe the numerical methods used to solve the PMCHWT formulation of eq. 25 both at the fundamental and at the SH frequency. In particular, we have exploited the Galerkin testing procedure to solve the singular SIEs, choosing the set of basis functions to coincide with the set of test functions [17].

Let us introduce a triangular mesh with N_e edges. We denote with \mathcal{M} the mesh surface, the length of the p^{th}

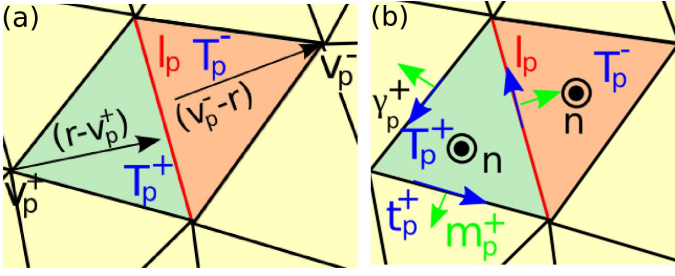


FIG. 1. (a) RWG basis function associated to the p^{th} edge and defined on the triangle pair T_p^+, T_p^- . In T_p^+ and T_p^- \mathbf{f}_p is proportional to the vector $(\mathbf{r} - \mathbf{v}_p^+)$ and $(\mathbf{v}_p^- - \mathbf{r})$, respectively. (b) For the triangle T_p^+ we show the support of the curve γ_p^+ its tangent vector \mathbf{t}_p^+ and binormal vector \mathbf{m}_p^+ .

edge as l_p , and the two triangles sharing the p^{th} edge as T_p^+ and T_p^- (Fig. 1 (a)). They have an area of A_p^+ and A_p^- respectively. The vertices of T_p^+ and T_p^- , which are opposite to the p^{th} edge, are indicated by v_p^+ and v_p^- respectively. The unknown electric and magnetic currents on \mathcal{M} are expanded in terms of the Rao-Wilton-Glisson (RWG) [18] functions set $\mathbf{f}_1, \mathbf{f}_2, \dots, \mathbf{f}_{N_e}$. The RWG function relative to the p^{th} edge is given by:

$$\mathbf{f}_p(\mathbf{r}) = \begin{cases} \mathbf{f}_p^+(\mathbf{r}) = +\frac{l_p}{2A_p^+} (\mathbf{r} - \mathbf{v}_p^+) & \mathbf{r} \in T_p^+ \\ \mathbf{f}_p^-(\mathbf{r}) = -\frac{l_p}{2A_p^-} (\mathbf{r} - \mathbf{v}_p^-) & \mathbf{r} \in T_p^- \\ \mathbf{0} & \text{otherwise} \end{cases}, \quad (28)$$

and the corresponding support is $S_p = T_p^+ \cup T_p^-$. We introduce also the symmetric product $\langle \mathbf{f}, \mathbf{g} \rangle = \int_S \mathbf{f} \cdot \mathbf{g} dS$ for the space of square integrable vector functions defined on S .

We assemble the discrete operators associated to $\mathcal{K}_l^{(\Omega, t)}$ and $\mathcal{T}_l^{(\Omega, t)}$ by projecting on the testing function \mathbf{f}_p the image through the operators $\mathcal{K}_l^{(\Omega, t)}$, and $\mathcal{T}_l^{(\Omega, t)}$ of the basis function \mathbf{f}_q . The above operators are explicitly derived in the section B of the appendix. Similarly, we assemble the discrete excitation vectors for both the fundamental and SH problem by projecting on the testing function \mathbf{f}_p the fields $\pi_0^{(\omega, e)}$, $\pi_0^{(\omega, m)}$, $\pi_e^{(2\omega)}$, $\pi_m^{(2\omega)}$, $\pi_b^{(2\omega)}$, $\mathbf{n} \times \pi_0^{(\omega, e)}$, $\mathbf{n} \times \pi_0^{(\omega, m)}$, $\mathbf{n} \times \pi_e^{(2\omega)}$, $\mathbf{n} \times \pi_m^{(2\omega)}$, and $\mathbf{n} \times \pi_b^{(2\omega)}$. In particular, in order to compute the quantities $\pi_e^{(2\omega)}$, $\pi_m^{(2\omega)}$, $\pi_b^{(2\omega)}$ we need to evaluate the fundamental field on the internal page of the surface S :

$$\mathbf{E}_i^{(\omega)}(\mathbf{r}) \Big|_{S_i} = \mathbf{E}_{i,t}^{(\omega)}(\mathbf{r}) \Big|_{S_i} + E_{i,n}^{(\omega)}(\mathbf{r}) \Big|_{S_i} \mathbf{n}, \quad (29)$$

where

$$\begin{aligned} \mathbf{E}_{i,t}^{(\omega)}(\mathbf{r}) \Big|_{S_i} &= -\mathbf{n} \times \mathbf{j}_i^{(\omega, m)}(\mathbf{r}), \\ E_{i,n}^{(\omega)}(\mathbf{r}) \Big|_{S_i} &= -j \frac{\nabla_S \cdot \mathbf{j}_i^{(\omega, e)}(\mathbf{r})}{\omega \varepsilon_i \{\omega\}}. \end{aligned} \quad (30)$$

Since the equivalent electric current $\mathbf{j}_i^{(\omega, e)}(\mathbf{r})$ are represented through the linear RWGs functions, $E_{i,n}^{(\omega)}(\mathbf{r})$ is a

piecewise constant function presenting a discontinuity of the first kind on the edges of the triangles. As a consequence, the calculation of the surface gradients $\nabla_S P_{S,n}^{(2\omega)}$, $\nabla_S P_{S,b}^{(2\omega)}$ needed to obtain $\pi_m^{(2\omega)}$, $\pi_b^{(2\omega)}$ has to be carried out in the framework of the distribution theory.

We now introduce the following notations. For each edge of the mesh, we define the two curves γ_p^+ and γ_p^- , having as support the perimeters of the triangles T_p^+ and T_p^- , respectively, and are oriented counterclockwise when viewed from the end of the vector \mathbf{n} ; \mathbf{t}_p^\pm are their tangent vectors, and $\mathbf{m}_p^\pm = \mathbf{t}_p^\pm \times \mathbf{n}$ are their binormal vectors (orthogonal to both \mathbf{t}_p^\pm and \mathbf{n}) (Fig. 1 (b)). The operators $\{\cdot\}|_{\gamma_{p,e}}$ and $\{\cdot\}|_{\gamma_{p,i}}$ associate to a given physical quantity defined on \mathcal{M} , with the exception of the mesh edges, its limiting value as the evaluation point approaches the curve γ_p^\pm from the external or the internal side of the triangle T_p^\pm , respectively.

The gradient of $P_{S,n}^{(2\omega)}$ on the support of the basis function \mathbf{f}_p , which is $S_p = T_p^+ \cup T_p^-$, has the following expression:

$$\nabla_S P_{S,n}^{(2\omega)} = \begin{cases} \left(P_{S,n}^{(2\omega)} \Big|_{\gamma_{p,e}^+} - P_{S,n}^{(2\omega)} \Big|_{\gamma_{p,i}^+} \right) \delta_{\gamma_p^+} \mathbf{m}_p^+ & \text{if } \mathbf{r} \in \gamma_p^+, \\ \left(P_{S,n}^{(2\omega)} \Big|_{\gamma_{p,e}^-} - P_{S,n}^{(2\omega)} \Big|_{\gamma_{p,i}^-} \right) \delta_{\gamma_p^-} \mathbf{m}_p^- & \text{if } \mathbf{r} \in \gamma_p^-, \\ \mathbf{0} & \text{if } \mathbf{r} \in \overset{\circ}{T}_p^+ \cup \overset{\circ}{T}_p^-, \end{cases} \quad (31)$$

where the functions $\delta_{\gamma_p^+}$ and $\delta_{\gamma_p^-}$ are Dirac function impulsive on the support of the curves γ_p^+ and γ_p^- , respectively, and 0 elsewhere on \mathcal{M} , such that $\iint_{\mathcal{M}} \delta_{\gamma_p^\pm} dS = 1$. It is worth noting that the first two branches of eq. 31 assume the same values along the edge l_p shared by the two triangles T_p^+ and T_p^- . The superficial current $\pi_m^{(2\omega)}$ on the support of \mathbf{f}_p will be:

$$\pi_m^{(2\omega)} = \begin{cases} \psi_m^+ \delta_{\gamma_p^+} & \text{if } \mathbf{r} \in \gamma_p^+, \\ \psi_m^- \delta_{\gamma_p^-} & \text{if } \mathbf{r} \in \gamma_p^-, \\ \mathbf{0} & \text{if } \mathbf{r} \in \overset{\circ}{T}_p^+ \cup \overset{\circ}{T}_p^-, \end{cases} \quad (32)$$

where the line currents ψ_m^\pm are defined as:

$$\begin{aligned} \psi_m^+ &= \frac{1}{\varepsilon_0} \left(P_{S,n}^{(2\omega)} \Big|_{\gamma_{p,e}^+} - P_{S,n}^{(2\omega)} \Big|_{\gamma_{p,i}^+} \right) \mathbf{t}_p^+, \\ \psi_m^- &= \frac{1}{\varepsilon_0} \left(P_{S,n}^{(2\omega)} \Big|_{\gamma_{p,e}^-} - P_{S,n}^{(2\omega)} \Big|_{\gamma_{p,i}^-} \right) \mathbf{t}_p^-, \end{aligned} \quad (33)$$

In conclusion, as a consequence of the linearity of the RWGs, the surface current $\pi_m^{(2\omega)}$ degenerates into line currents ψ_m^\pm defined on the mesh's edges, directed along the edge itself.

Similarly, in order to compute the magnetic surface currents $\boldsymbol{\pi}_b^{(2\omega)}$ introduced in eq. 13, we need to calculate the gradient of $P_{b,n}^{(2\omega)}$. $P_{b,n}^{(2\omega)}$ is a piecewise quadratic function presenting a discontinuity of the first kind along the mesh edges. Therefore, we can repeat the derivation of the previous paragraph, obtaining:

$$\boldsymbol{\pi}_b^{(2\omega)} = \begin{cases} \boldsymbol{\psi}_b^+ \delta_{\gamma_p^+} & \text{if } \mathbf{r} \in \gamma_p^+, \\ \boldsymbol{\psi}_b^- \delta_{\gamma_p^-} & \text{if } \mathbf{r} \in \gamma_p^-, \\ \frac{1}{\varepsilon_0} \mathbf{n} \times \nabla_S P_{S,b}^{(2\omega)} & \text{if } \mathbf{r} \in \overset{\circ}{T}_p^+ \cup \overset{\circ}{T}_p^-, \end{cases} \quad (34)$$

where

$$\begin{aligned} \boldsymbol{\psi}_b^+ &= \frac{1}{\varepsilon_0} \left(P_{S,b}^{(2\omega)} \Big|_{\gamma_{p,e}^+} - P_{S,b}^{(2\omega)} \Big|_{\gamma_{p,i}^+} \right) \mathbf{t}_p^+, \\ \boldsymbol{\psi}_b^- &= \frac{1}{\varepsilon_0} \left(P_{S,b}^{(2\omega)} \Big|_{\gamma_{p,e}^-} - P_{S,b}^{(2\omega)} \Big|_{\gamma_{p,i}^-} \right) \mathbf{t}_p^-. \end{aligned} \quad (35)$$

Thus, the current $\boldsymbol{\pi}_b^{(2\omega)}$ is a superposition of surface currents defined on the interior of the mesh's triangles and of line currents $\boldsymbol{\psi}_b^\pm$ defined on the mesh's edges and directed along the edge itself. The line currents have not been considered in [13], as a result the provided expression of the discrete excitation vector associated to $\langle \mathbf{f}_p, \boldsymbol{\pi}_m^{(2\omega)} \rangle$ is incorrect. In the appendix C all the discrete excitation vectors are explicitly calculated.

V. DISCUSSION

In the first part of this section, we validate our formulation for the problem of the SH generation from an isolated gold sphere using the full wave SH Mie solution (SH-Mie) of the problems 2 and 12. The SH-Mie solution has been obtained by expanding the pump field, the non-linear sources and the SH fields in series of vector spherical wave functions [15]. Then, we investigate the SH generation properties of a triangular nano-prism. The scatterers are homogeneous gold particles, embedded in air. The investigated physical quantity is the SH radiated power per unit solid angle collected along the direction \mathbf{k}

$$dP^{(\Omega)}/d\Omega(\mathbf{k}) = \lim_{\|\mathbf{r}\| \rightarrow +\infty} \left[\frac{r^2}{2\zeta_e \{\Omega\}} \left\| \mathbf{E}_e^{(\Omega)}(\mathbf{k}) \right\|^2 \right]. \quad (36)$$

From both theoretical and experimental studies it results that the component $\chi_{\perp\parallel\parallel}^{(2)}$ only weakly contributes to the SH generation from noble metals [16, 19]. Following Bachelier *et al.* [19] we express the parameters $\chi_{\perp\perp\perp}^{(2)}$, $\chi_{\parallel\perp\parallel}^{(2)}$, and $\gamma^{(2)}$ through the dimensionless *phenomenological Rudnick-Stern parameters* a , b and d [20], as follows:

$$\left[\chi_{\perp\perp\perp}^{(2)}, \chi_{\parallel\perp\parallel}^{(2)}, \gamma^{(2)} \right] = - \left[\frac{a}{4}, \frac{b}{2}, \frac{d}{8} \right] \chi_b^{(1)}(\omega) \frac{\omega_p^2 \varepsilon_0}{\omega^2 \varepsilon n_0}, \quad (37)$$

where $\chi_b^{(1)}(\omega) = (\varepsilon_i(\omega)/\varepsilon_0 - 1)$ is the bulk linear susceptibility of the metal, e is the electron charge (absolute value), n_0 is the number density of the conduction electrons, ω_p is the plasma frequency and ε_0 is the permittivity of the vacuum. By choosing $a = 1$, $b = -1$ and $d = 1$ we obtain the Rudnick-Stern hydrodynamic model [20]. The gold dispersion is modeled by fitting experimental data [21]. The integrals involved in the numerical solution have been evaluated using four Gauss quadrature points for each triangle of \mathcal{M} , and their singularities have been managed exploiting singularity extraction techniques [22].

The gold sphere is excited by a plane wave of unitary intensity, namely $\mathbf{E}_0^{(\omega)} = \exp(-j\omega\sqrt{\varepsilon_e\mu_e z}) \hat{\mathbf{x}}$ propagating along the positive direction of the z -axis and linearly polarized along x . The exciting wavelength corresponds to the plasmonic resonance of a gold spherical particle in the Rayleigh limit, *i.e.* $520nm$. The relative permittivity used in the calculations are $\varepsilon_i(520nm) = -3.88 - 2.63j$ and $\varepsilon_i(260nm) = -1.20 - 4.67j$ for the fundamental and the SH problem, respectively. The mesh has a number of edges equal to $N_e = 3747$. The maximum expansion order of vector spherical wave functions, used in the calculation of the SH-Mie solution, is $N = 10$. Aiming at an accurate validation of the proposed approach, we show in fig. 2 the quantity $dP^{(2\omega)}/d\Omega$ as a function of the inclination angle θ for $\phi = 0$ and $\phi = 90$. These quantities have been calculated by the SH-Mie (orange triangles for $\phi = 0$ and red circles for $\phi = 90$) and by the SH-SIE (continuous black line for $\phi = 0$ and continuous blue line for $\phi = 90$). Several sphere's diameters D have been considered: the first row of fig. 2 (panels a-d), is relative to an electrically small particle with $D = 20nm$, the second row (e-h) to $D = 100nm$, the third row (i-l) to $D = 200nm$. We considered in the first three columns only one SH source at a time, whereas in the fourth column the different nonlinear polarization sources are simultaneously active. In particular, in the first column of fig. 2, corresponding to panels (a,e,i), we considered only the nonlocal-bulk source $P_{b,n}^{(2\omega)}$ using the coefficients $(\gamma, \chi_{\parallel\perp\parallel}^{(2)}, \chi_{\perp\perp\perp}^{(2)}) = (1, 0, 0)$. In the second column (b,f,j) only the surface source $P_{S,t}^{(2\omega)}$ has been considered assuming $(\gamma, \chi_{\parallel\perp\parallel}^{(2)}, \chi_{\perp\perp\perp}^{(2)}) = (0, 1, 0)$, whereas in the third column (c,g,k) only the surface source $P_{S,n}^{(2\omega)}$ has been considered assuming $(\gamma, \chi_{\parallel\perp\parallel}^{(2)}, \chi_{\perp\perp\perp}^{(2)}) = (0, 0, 1)$. Eventually, in panels (d,h,l,p) we considered a realistic physical case in which the different weights are calculated using eq. 37 with $(a, b, d) = (1, -1, 1)$. In all the different cases shown in fig. 2 very good agreement between the SH-SIE and the SH-Mie formulations can be found.

In Fig. 3 we calculate the relative error ξ of the SH-SIE formulation with respect to the SH-Mie formulation, defined as:

$$\xi = \left(dP^{(2\omega)}/d\Omega - P_{\text{MIE}}^{(2\omega)}/d\Omega \right) / \left(P^{(2\omega)}/d\Omega \right), \quad (38)$$

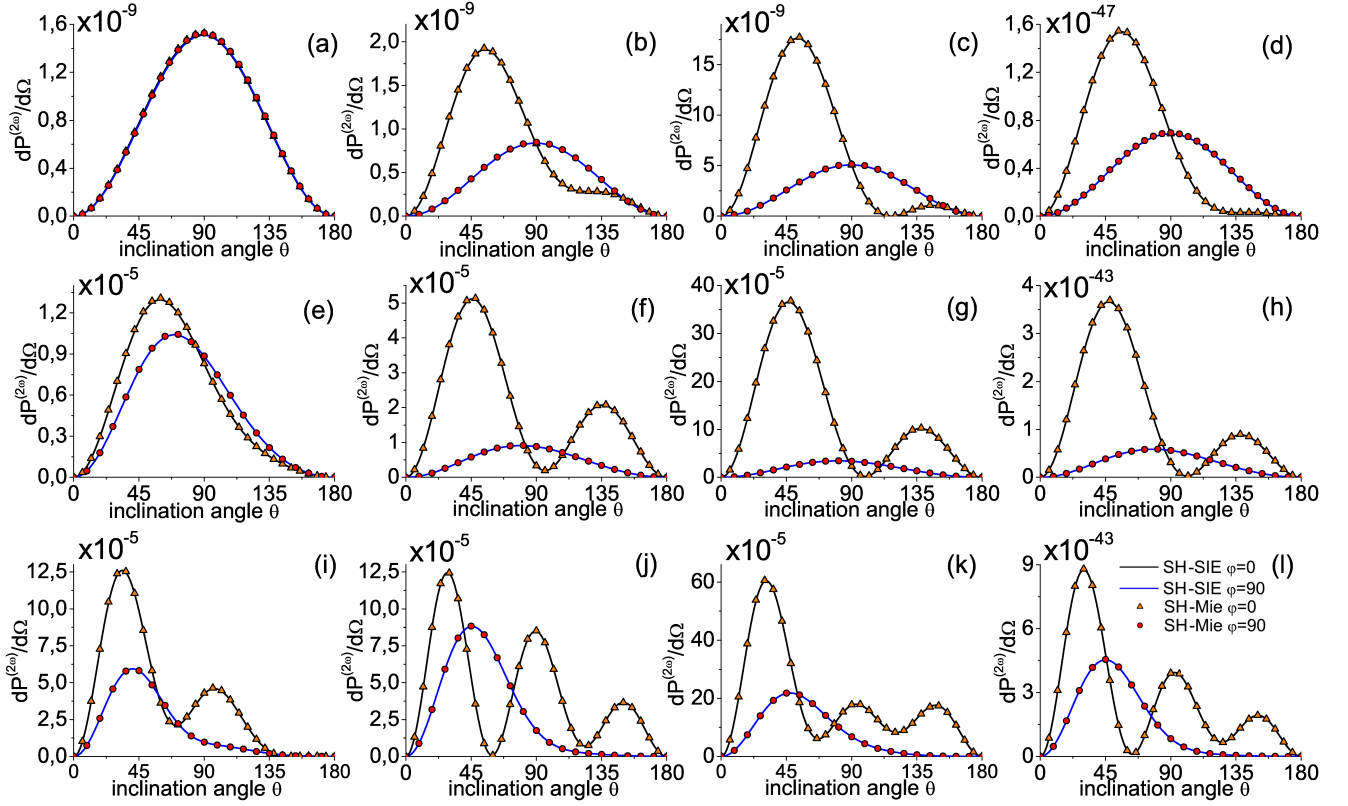


FIG. 2. SH radiated power per unit solid angle (expressed in Watt/Steradian) of a gold sphere with diameter (a-d) 20nm, (e-h) 100nm (i-l) 200nm. Different combinations of SHG polarization sources have been considered, namely $(\gamma^{(2)}, \chi_{\parallel\perp\parallel}^{(2)}, \chi_{\perp\perp\perp}^{(2)}) = (1, 0, 0)$ in panels (a,e,i); $(0, 1, 0)$ in panels (b,f,j); $(0, 0, 1)$ in panels (c,g,k). In panels (d,h,l,p) the sources have been weighted using eq. 37 with $(a, b, d) = (1, -1, 1)$. The sphere is excited by a x-polarized plane wave of unitary intensity propagating along the positive z axis with wavelength 520nm. The diagrams are in linear scale.

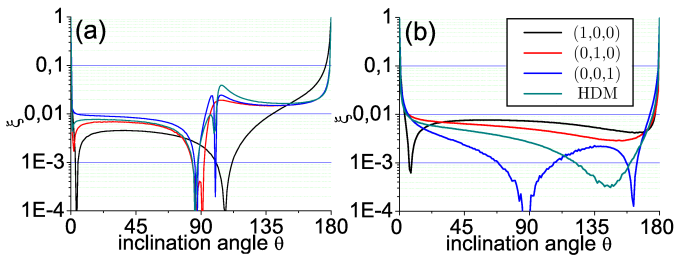


FIG. 3. Relative error of $dP^{(2\omega)}/d\Omega$ calculated with the SH-SIE with respect to the SH-Mie solution for a sphere of diameter $D = 100nm$ as a function of the inclination angle θ for (a) $\phi = 0$ and (b) $\phi = 90$. Different combinations of SHG polarization sources have been considered, namely $(\gamma^{(2)}, \chi_{\parallel\perp\parallel}^{(2)}, \chi_{\perp\perp\perp}^{(2)}) = (1, 0, 0)$ (black line); $(0, 1, 0)$ (red line); $(0, 0, 1)$ (blue line); the hydrodynamic model of eq. 37 with $(a, b, d) = (1, -1, 1)$ (green line).

where $P_{MIE}^{(2\omega)}/d\Omega$ is the radiated power per unit solid angle calculate with the SH-Mie formulation. The error is plotted as a function of inclination angle θ for (a) $\phi = 0$ and (b) $\phi = 90$ for of the for the $D = 100nm$ sphere. All

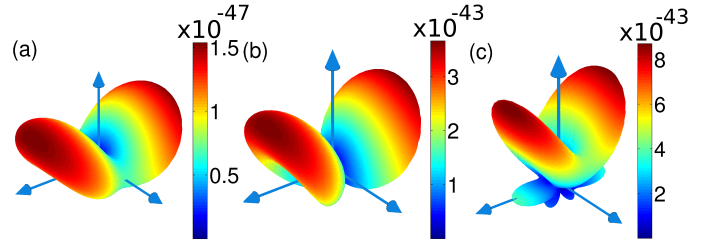


FIG. 4. Radiation diagram of $dP^{(2\omega)}/d\Omega$ (expressed in Watt/Steradian) for a gold sphere with diameter: (a) 20nm, (b) 100nm (c) 200nm. The sphere is excited by a x-polarized plane wave of unitary intensity propagating along the positive direction of the z -axis with wavelength 520nm. The radiated powe is evaluated at 260nm. The diagrams are in linear scale. The sources have been weighted using eq. 37 with $(a, b, d) = (1, -1, 1)$.

the investigated cases present a comparable error, below 3%. Only in correspondence of the forward and backward scattering direction, when the corresponding value of $dP^{(2\omega)}/d\Omega$ is very small the error is higher.

In figure 4 we show the radiation diagram of $dP^{(2\omega)}/d\Omega$

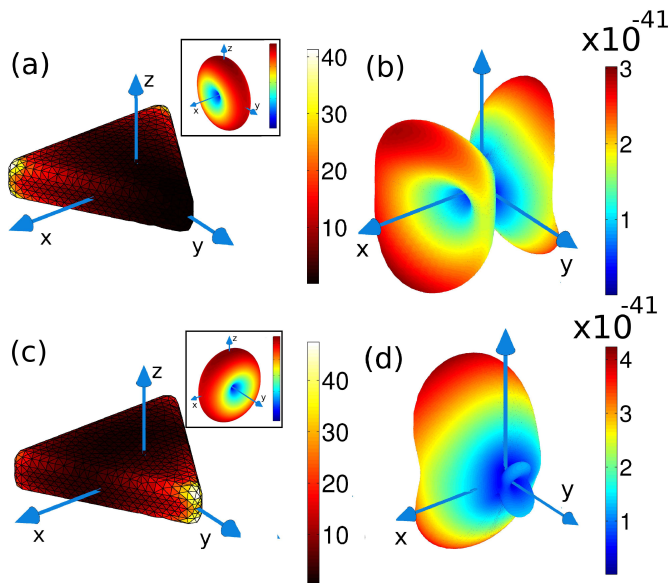


FIG. 5. (a,c) Magnitude of the fundamental $\mathbf{E}_c^{(\omega)}$ at the fundamental frequency on the surface of the triangular nano-prism excited by a monochromatic ($\lambda = 690nm$) plane wave of unitary intensity propagating along the positive z - axis and linearly polarized along (a) x and (c) y , and corresponding radiated power per unit solid angle (inset). (b,d) Radiation diagram of $dP^{(2\omega)}/d\Omega$ (expressed in Watt/Steradian) for both a (b) x-polarized (d) y-polarized pump. The sources have been weighted using eq. 37 with $(a, b, d) = (1, -1, 1)$.

for different diameters of the sphere, $D =$ (a) $20nm$ (b) $100nm$ (c) $200nm$. The SH radiated power vanishes for the forward and backscattering directions for all the investigated diameters, because the sphere is rotationally symmetric around the propagation direction. As we increase the sphere's diameter we notice the appearance of multiple oscillations corresponding to high order modes. Moreover, as the particle size increases, the inclination angle corresponding to the first maximum SH intensity approaches the forward scattering direction. This behavior has been experimentally demonstrated for silver spherical particles in a recent work by Gonella *et al.* [23].

We now consider a triangular nano-prism of height $h = 40nm$ with rounded edges of length $200nm$. The radius of the osculating cylinder (sphere) at each edge (corner) is $10nm$. This shape is of extreme interest in nanoplasmonics as the building block of bow-tie nano-antennas, whose SH properties have been recently investigated in [24]. We chose as the exciting wavelength $\lambda = 690nm$, corresponding to the peak of the extinction cross section over the visible range. We first analyze the scattering properties at the fundamental frequency. In figure 5 (a,c) we show the magnitude of the total electric field at the fundamental frequency on the surface of the triangular nano-prism when the incident plane wave is polarized along (a) the x axis and (c) the y axis. When the incident plane wave is x-polarized

two *hot spots* arise at the two ends of the edge parallel to the incident polarization, whereas in correspondence of a y-polarized excitation the remaining corner experiences the highest field enhancement. The radiated power $dP^{(\omega)}/d\Omega$ at the fundamental frequency can be attributed to an electric dipole oriented along the polarization direction (inset of Fig. 5 (a,c)). In panels (b,d) we study the SH radiated power $dP^{(2\omega)}/d\Omega$ by the triangular nano-prism. The different sources are weighted using eq. 37 with $(a, b, d) = (1, -1, 1)$. Unlike the linear scattering, $dP^{(2\omega)}/d\Omega$ shows a richer behavior dominated by higher order modes. Moreover, as the analyzed nano-prism is not rotationally symmetric around the propagation direction, the radiated power in both the forward and backscattering directions is non zero. Furthermore, the shape of $dP^{(2\omega)}/d\Omega$ is affected by the distribution of the electric field on the surface of the particle, shown in fig. 5 (a,b). In fact, we attribute the presence of the two lobes in panel to the strong field localization that occurs in correspondence of the two corners of the edge of the triangular-nanoprism parallel to x-axis. In contrast, when the incident field is directed along the y-axis, the radiation diagram features one lobe driven by the hot-spot on the remaining corner. Although both the surface area and the volume of the nano-prisms are lower than those of the sphere of diameter $200nm$ investigated earlier, the maximum intensity of SH radiated power per unit solid angle $dP^{(2\omega)}/d\Omega$ of the nano-prism (Fig. 5(b,d)) is almost two order of magnitude higher compared to the sphere (Fig. 4 (b)). This fact is due to both the higher values of the non-linear susceptibilities of gold at $690nm$ and to the NP asymmetric shape [25].

VI. CONCLUSIONS

We have presented a surface integral equation method to accurately solve the second harmonic generation problem in metal nanoparticles with arbitrary shapes accounting for both the nonlocal-bulk and local-surface nonlinear polarization sources. We have demonstrated that the contribution of the nonlocal-bulk nonlinear polarization source to the SH electromagnetic field can be taken into account by introducing an equivalent surface magnetic current on the nanoparticle boundary. We compared the numerical solution of the SH surface integral equations to the analytical Mie solution for spheres of several radii, obtaining very good agreement for any investigated case. The present treatment could also be easily extended to modeling sum-frequency and higher harmonic generation. The developed method paves the way to a better understanding of the process of SHG in arbitrarily shaped nanoparticles. This approach can have a high impact in the design of novel nanoplasmonic devices with enhanced SHG emission, including for instance sensor probing physical and chemical properties of material surfaces.

VII. ACKNOWLEDGEMENT

This work was partly supported by the Italian Ministry of Education, University and Research through the project PON01_02782.

Appendix A: Electromagnetic field generated by surface sources

In the present section, we provide the expression of the electromagnetic field generated by a surface distribution of electric and magnetic currents ($\mathbf{j}^{(\Omega,e)}, \mathbf{j}^{(\Omega,m)}$) defined on S and radiating in a homogeneous medium with constitutive parameters ($\varepsilon_l \{\Omega\}, \mu_l$) at frequency Ω . The electromagnetic field radiated by both the electric and magnetic magnetic currents is:

$$\mathbf{E}^{(\Omega)}(\mathbf{r}) = \mathcal{E}_l^{(\Omega)} \left\{ \mathbf{j}^{(\Omega,e)}, \mathbf{j}^{(\Omega,m)} \right\}(\mathbf{r}) \quad (\text{A1a})$$

$$\mathbf{H}^{(\Omega)}(\mathbf{r}) = \mathcal{H}_l^{(\Omega)} \left\{ \mathbf{j}^{(\Omega,e)}, \mathbf{j}^{(\Omega,m)} \right\}(\mathbf{r}) \quad (\text{A1b})$$

where:

$$\begin{aligned} \mathcal{E}_l^{(\Omega)} \left\{ \mathbf{j}^{(\Omega,e)}, \mathbf{j}^{(\Omega,m)} \right\} &= \zeta_l \{\Omega\} \mathcal{T}_l^{(\Omega)} \left\{ \mathbf{j}^{(\Omega,e)} \right\} + \mathcal{K}_l^{(\Omega)} \left\{ \mathbf{j}^{(\Omega,m)} \right\} + \begin{cases} \mathbf{0} & \text{if } \mathbf{r} \notin S, \\ + \frac{\zeta_l \{\Omega\}}{2jk_l \{\Omega\}} [\nabla_S \cdot \mathbf{j}^{(\Omega,e)}] \mathbf{n} - \frac{1}{2} \mathbf{n} \times \mathbf{j}^{(\Omega,m)} & \text{if } \mathbf{r} \in S_i, \\ - \frac{\zeta_l \{\Omega\}}{2jk_l \{\Omega\}} [\nabla_S \cdot \mathbf{j}^{(\Omega,e)}] \mathbf{n} + \frac{1}{2} \mathbf{n} \times \mathbf{j}^{(\Omega,m)} & \text{if } \mathbf{r} \in S_e, \end{cases} \\ \mathcal{H}_l^{(\Omega)} \left\{ \mathbf{j}^{(\Omega,e)}, \mathbf{j}^{(\Omega,m)} \right\} &= -\mathcal{K}_l^{(\Omega)} \left\{ \mathbf{j}^{(\Omega,e)} \right\} + \frac{\mathcal{T}_l^{(\Omega)} \left\{ \mathbf{j}^{(\Omega,m)} \right\}}{\zeta_l \{\Omega\}} + \begin{cases} \mathbf{0} & \text{if } \mathbf{r} \notin S, \\ + \frac{1}{2} \mathbf{n} \times \mathbf{j}^{(\Omega,e)}(\mathbf{r}) + \frac{[\nabla_S \cdot \mathbf{j}^{(\Omega,m)}(\mathbf{r})]}{2j\zeta_l \{\Omega\} k_l \{\Omega\}} \mathbf{n} & \text{if } \mathbf{r} \in S_i, \\ - \frac{1}{2} \mathbf{n} \times \mathbf{j}^{(\Omega,e)}(\mathbf{r}) - \frac{[\nabla_S \cdot \mathbf{j}^{(\Omega,m)}(\mathbf{r})]}{2j\zeta_l \{\Omega\} k_l \{\Omega\}} \mathbf{n} & \text{if } \mathbf{r} \in S_e, \end{cases} \end{aligned} \quad (\text{A2})$$

$\nabla_S \cdot$ denotes the surface divergence, \mathcal{K}_l and \mathcal{T}_l denote the integral operators:

$$\mathcal{K}_l^{(\Omega)} \{ \mathbf{w} \}(\mathbf{r}) = - \int_S \mathbf{w}(\mathbf{r}') \times \nabla' g_l^{(\Omega)}(\mathbf{r} - \mathbf{r}') dS' \quad (\text{A3a})$$

$$\begin{aligned} \mathcal{T}_l^{(\Omega)} \{ \mathbf{w} \}(\mathbf{r}) &= -jk_l \{\Omega\} \int_S g_l^{(\Omega)}(\mathbf{r} - \mathbf{r}') \mathbf{w}(\mathbf{r}') dS' + \\ &- \frac{1}{jk_l \{\Omega\}} \int_S \nabla' g_l^{(\Omega)}(\mathbf{r} - \mathbf{r}') \nabla'_S \cdot \mathbf{w}(\mathbf{r}') dS' \end{aligned} \quad (\text{A3b})$$

$g_l^{(\Omega)}$ is the homogeneous space Green's function, *i.e.* $g_l^{(\Omega)}(\mathbf{r} - \mathbf{r}') = \frac{e^{-jk_l \{\Omega\} |\mathbf{r} - \mathbf{r}'|}}{4\pi |\mathbf{r} - \mathbf{r}'|}$, $k_l \{\Omega\} = \Omega \sqrt{\mu_l \varepsilon_l \{\Omega\}}$.

$$\mathcal{K}_l^{(\Omega,t)} \{ \cdot \} = -\mathbf{n} \times \mathbf{n} \times \mathcal{K}_l^{(\Omega)} \{ \cdot \} \Big|_{S_l} \quad (\text{A4a})$$

$$\mathcal{T}_l^{(\Omega,t)} \{ \cdot \} = -\mathbf{n} \times \mathbf{n} \times \mathcal{T}_l^{(\Omega)} \{ \cdot \} \Big|_{S_l}. \quad (\text{A4b})$$

Appendix B: Discrete Operators

By projecting on the testing function \mathbf{f}_p the image through the operators $\mathcal{K}_l^{(\Omega,t)}$ of the basis function \mathbf{f}_q we

obtain:

$$\begin{aligned} \langle \mathbf{f}_p, \mathcal{K}_l^{(\Omega,t)} \mathbf{f}_q \rangle &= \frac{l_p l_q}{4} \sum_{r=\pm} \sum_{s=\pm} \frac{r s}{A_p^r A_q^s} \iint_{T_p^r} (\mathbf{r} - \mathbf{v}_p^r) \cdot \\ &\left[\iint_{T_q^s} (\mathbf{r}' - \mathbf{v}_q^s) \times \nabla g_l^{(\Omega)}(\mathbf{r} - \mathbf{r}') dS' \right] dS \end{aligned} \quad (\text{B1})$$

Similarly, by projecting on the testing function \mathbf{f}_p the image of the basis function \mathbf{f}_q through the operators $\mathcal{T}_l^{(\Omega,t)}$ we obtain:

$$\begin{aligned} \langle \mathbf{f}_p, \mathcal{T}_l^{(\Omega,t)} \mathbf{f}_q \rangle &= -l_p l_q \sum_{r=\pm} \sum_{s=\pm} \frac{r s}{A_p^r A_q^s} \times \\ &\times \left[\frac{jk_l \{\Omega\}}{4} \iint_{T_p^r} (\mathbf{r} - \mathbf{v}_p^r) \cdot \iint_{T_q^s} g_l^{(\Omega)}(\mathbf{r} - \mathbf{r}') (\mathbf{r} - \mathbf{v}_q^s) dS' dS \right. \\ &\left. + \frac{1}{jk_l \{\Omega\}} \iint_{T_p^r} \iint_{T_q^s} g_l^{(\Omega)}(\mathbf{r} - \mathbf{r}') dS' dS \right] \end{aligned} \quad (\text{B2})$$

Appendix C: Excitation Vectors

The discrete excitation vector associated to the superficial electric current density $\boldsymbol{\pi}_e^{(2\omega)}$ is:

$$\begin{aligned} \langle \mathbf{f}_p, \mathbf{n} \times \boldsymbol{\pi}_e^{(2\omega)} \rangle &= \iint_{S_p} \mathbf{f}_p \cdot \mathbf{n} \times \boldsymbol{\pi}_e^{(2\omega)} dS = \\ &- j2\omega \sum_{r=\pm} \iint_{T_p^r} \mathbf{P}_{S,t}^{(2\omega)} \cdot \mathbf{n} \times \mathbf{f}_p^r dS \quad (\text{C1}) \end{aligned}$$

where we have split the integral domain S_p into the two constitutive triangular facets T_p^\pm .

We now assembly the discrete excitation vector associated to the superficial magnetic current density $\boldsymbol{\pi}_m^{(2\omega)}$:

$$\langle \mathbf{f}_p, \mathbf{n} \times \boldsymbol{\pi}_m^{(2\omega)} \rangle = \iint_{S_p} \mathbf{f}_p \cdot \mathbf{n} \times \boldsymbol{\pi}_m^{(2\omega)} dS \quad (\text{C2})$$

Splitting the integral domain S_p into the two constitutive triangular facets T_p^\pm and using the expression of $\boldsymbol{\pi}_m^{(2\omega)}$ given in eq. 32, we obtain:

$$\begin{aligned} \langle \mathbf{f}_p, \mathbf{n} \times \boldsymbol{\pi}_m^{(2\omega)} \rangle &= \\ \frac{1}{2} \oint_{\gamma_p^+} \mathbf{f}_p^+ \cdot \mathbf{n} \times \boldsymbol{\psi}_m^+ dl + \frac{1}{2} \oint_{\gamma_p^-} \mathbf{f}_p^- \cdot \mathbf{n} \times \boldsymbol{\psi}_m^- dl \quad (\text{C3}) \end{aligned}$$

where we have used the sampling property of δ_p^\pm , when they are applied to the discontinuous function $\mathbf{f}_p(\mathbf{r})$, which is \mathbf{f}_p^\pm in T_p^\pm , and $\mathbf{0}$ elsewhere. Using the definition of $\boldsymbol{\psi}_m^\pm$ given in eq. 33 we obtain:

$$\begin{aligned} \langle \mathbf{f}_p, \mathbf{n} \times \boldsymbol{\pi}_m^{(2\omega)} \rangle &= \\ - \frac{1}{2\varepsilon_0} \oint_{\gamma_p^+} \mathbf{f}_p^+ \cdot \mathbf{m}_p^+ \left[P_{S,n}^{(2\omega)}|_{\gamma_{p,e}^+} - P_{S,n}^{(2\omega)}|_{\gamma_{p,i}^+} \right] dl + \\ - \frac{1}{2\varepsilon_0} \oint_{\gamma_p^-} \mathbf{f}_p^- \cdot \mathbf{m}_p^- \left[P_{S,n}^{(2\omega)}|_{\gamma_{p,e}^-} - P_{S,n}^{(2\omega)}|_{\gamma_{p,i}^-} \right] dl \quad (\text{C4}) \end{aligned}$$

The quantities $\mathbf{f}_p^\pm \cdot \mathbf{m}_p^\pm$ vanish on γ_p^\pm except on the common edge l_p , where they are equal to ± 1 . Therefore, we have:

$$\langle \mathbf{f}_p, \mathbf{n} \times \boldsymbol{\pi}_m^{(2\omega)} \rangle = \frac{l_p}{\varepsilon_0} \left[P_{S,n}^{(2\omega)}|_{T_p^+} - P_{S,n}^{(2\omega)}|_{T_p^-} \right] \quad (\text{C5})$$

where we have exploited the fact that $P_{S,n}^{(2\omega)}|_{\gamma_{p,i}^\pm} = P_{S,n}^{(2\omega)}|_{\gamma_{p,e}^\pm} = P_{S,n}^{(2\omega)}|_{T_p^\pm}$, and $P_{S,n}^{(2\omega)}|_{T_p^\pm}$ is the value of function $P_{S,n}^{(2\omega)}$ in the interior of T_p^\pm .

Then, we derive the expression for the discrete excitation vector associated to the superficial magnetic current density $\boldsymbol{\pi}_b^{(2\omega)}$:

$$\langle \mathbf{f}_p, \mathbf{n} \times \boldsymbol{\pi}_b^{(2\omega)} \rangle = \iint_{S_p} \mathbf{f}_p(\mathbf{r}) \cdot \mathbf{n} \times \boldsymbol{\pi}_b^{(2\omega)} dS \quad (\text{C6})$$

The current $\boldsymbol{\pi}_b^{(2\omega)}$ is a superposition of surface currents defined on the interior of the mesh's triangles and of line currents $\boldsymbol{\psi}_b^\pm$ as exemplified in eq. 34:

$$\begin{aligned} \langle \mathbf{f}_p, \mathbf{n} \times \boldsymbol{\pi}_b^{(2\omega)} \rangle &= I_1 + I_2 = \frac{1}{2} \sum_{r=\pm} \oint_{\gamma_p^r} \mathbf{f}_p^r \cdot \mathbf{n} \times \boldsymbol{\psi}_b^r dl + \\ &- \frac{1}{\varepsilon_0} \sum_{r=\pm} \iint_{T_p^r} \mathbf{f}_p^r \cdot \nabla_S P_{b,n}^{(2\omega)} dS \quad (\text{C7}) \end{aligned}$$

The evaluation of the integral I_1 follows the same steps of $\langle \mathbf{f}_p, \mathbf{n} \times \boldsymbol{\pi}_m^{(2\omega)} \rangle$. To evaluate the term I_2 , we first apply the vectorial identity $\mathbf{f}_p^r \cdot \nabla_S P_{b,n}^{(2\omega)} = \nabla_S \cdot \left[P_{b,n}^{(2\omega)} \mathbf{f}_p^r \right] - P_{b,n}^{(2\omega)} \nabla_S \cdot \mathbf{f}_p^r$, then the divergence theorem on the first of the two resulting terms, obtaining:

$$\begin{aligned} I_2 &= -\frac{1}{\varepsilon_0} \sum_{r=\pm} \oint_{\gamma_p^r} P_{b,n}^{(2\omega)} \Big|_{\gamma_{p,i}^r} \mathbf{f}_p^r \cdot \mathbf{m}_p^r dl \\ &+ \frac{1}{\varepsilon_0} \sum_{r=\pm} \iint_{T_p^r} P_{b,n}^{(2\omega)} \nabla_S \cdot \mathbf{f}_p^r dS \quad (\text{C8}) \end{aligned}$$

The first term on the r.h.s. of eq. C8 is equal and opposite to I_1 therefore they cancel in eq. C7, *i.e.*

$$\langle \mathbf{f}_p, \mathbf{n} \times \boldsymbol{\pi}_b^{(2\omega)} \rangle = +\frac{1}{\varepsilon_0} l_p \sum_{r=\pm} \left(\frac{r}{A_p^r} \right) \iint_{T_p^r} P_{b,n}^{(2\omega)} dS \quad (\text{C9})$$

Now we now assembly the discrete excitation vector associated to the vector field $\mathbf{n} \times \boldsymbol{\pi}_e^{(2\omega)}$

$$\begin{aligned} \langle \mathbf{f}_p, \boldsymbol{\pi}_e^{(2\omega)} \rangle &= \iint_{S_p} \mathbf{f}_p \cdot \boldsymbol{\pi}_e^{(2\omega)} dS = \\ &j2\omega \sum_{r=\pm} \iint_{T_p^r} \mathbf{f}_p^r \cdot \mathbf{P}_{S,t}^{(2\omega)} dS \quad (\text{C10}) \end{aligned}$$

Then, we calculate the discrete excitation vector associated to the superficial vector field $\mathbf{n} \times \boldsymbol{\pi}_m^{(2\omega)}$:

$$\langle \mathbf{f}_p, \boldsymbol{\pi}_m^{(2\omega)} \rangle = \iint_{S_p} \mathbf{f}_p \cdot \boldsymbol{\pi}_m^{(2\omega)} dS \quad (\text{C11})$$

Splitting the integral domain S_p into the two constitutive triangular facets T_p^\pm , and using eq. 32 we have:

$$\langle \mathbf{f}_p, \boldsymbol{\pi}_m^{(2\omega)} \rangle = \frac{1}{2} \oint_{\gamma_p^+} \mathbf{f}_p^+ \cdot \boldsymbol{\psi}_m^+ dl + \frac{1}{2} \oint_{\gamma_p^-} \mathbf{f}_p^- \cdot \boldsymbol{\psi}_m^- dl \quad (\text{C12})$$

Using the eq. 33 we obtain:

$$\begin{aligned} \langle \mathbf{f}_p, \boldsymbol{\pi}_m^{(2\omega)} \rangle &= \frac{1}{2\varepsilon_0} \sum_{r=\pm} \oint_{\gamma_p^r} P_{S,n}^{(2\omega)}|_{\gamma_{p,e}^r} \mathbf{f}_p^r \cdot \mathbf{t}_p^r dl \\ &- \frac{1}{2\varepsilon_0} \sum_{r=\pm} P_{S,n}^{(2\omega)}|_{\gamma_{p,i}^r} \oint_{\gamma_p^r} \mathbf{f}_p^r \cdot \mathbf{t}_p^r dl \quad (\text{C13}) \end{aligned}$$

where we have used the fact that $P_{S,n}^{(2\omega)}|_{\gamma_{p,i}^\pm}$ is constant along γ_p^\pm . By noting that $\oint_{\gamma_p^r} \mathbf{f}_p^r \cdot \mathbf{t}_p^r dl = 0$, we eventually obtain:

$$\langle \mathbf{f}_p, \boldsymbol{\pi}_m^{(2\omega)} \rangle = \frac{1}{2\varepsilon_0} \sum_{r=\pm} \oint_{\gamma_p^r} P_{S,n}^{(2\omega)}|_{\gamma_{p,e}^r} \mathbf{f}_p^r \cdot \mathbf{t}_p^r dl \quad (\text{C14})$$

The integral in eq. C14 can be evaluated analytically.

We now assemble the discrete excitation vector associated to $\mathbf{n} \times \boldsymbol{\pi}_b^{(2\omega)}$:

$$\langle \mathbf{f}_p, \boldsymbol{\pi}_b^{(2\omega)} \rangle = \iint_{S_p} \mathbf{f}_p \cdot \boldsymbol{\pi}_b^{(2\omega)} dS \quad (\text{C15})$$

Splitting the integral domain S_p into the two constitutive triangular facets T_p^\pm and using eq. 34 we have:

$$\begin{aligned} \langle \mathbf{f}_p, \boldsymbol{\pi}_b^{(2\omega)} \rangle &= I_1 + I_2 = \frac{1}{2} \sum_{r=\pm} \oint_{\gamma_p^r} \mathbf{f}_p^r \cdot \boldsymbol{\psi}_b^r dl \\ &\quad - \frac{1}{\varepsilon_0} \sum_{r=\pm} \iint_{T_p^r} \mathbf{n} \times \mathbf{f}_p^r \cdot \nabla_S P_{b,n}^{(2\omega)} dS \end{aligned} \quad (\text{C16})$$

By using eq. 35, the evaluation of the integral I_1 follows the same steps of $\langle \mathbf{f}_p, \boldsymbol{\pi}_m^{(2\omega)} \rangle$:

$$I_1 = \frac{1}{2\varepsilon_0} \sum_{r=\pm} \oint_{\gamma_p^r} \mathbf{f}_p^r \cdot \mathbf{t}_p^r \left(P_{b,n}^{(2\omega)}|_{\gamma_{p,e}^r} - P_{b,n}^{(2\omega)}|_{\gamma_{p,i}^r} \right) dl \quad (\text{C17})$$

Concerning the term I_2 , we can apply the vectorial identity $[\mathbf{n} \times \mathbf{f}_p^r] \cdot \nabla_S P_{b,n}^{(2\omega)} = \nabla_S \cdot [P_{b,n}^{(2\omega)} (\mathbf{n} \times \mathbf{f}_p^r)]$ because the quantity $\nabla_S \cdot [\mathbf{n} \times \mathbf{f}_p^r]$ vanishes in T_p^r . Then, by using the divergence theorem on the resulting integral, we obtain:

$$I_2 = \frac{1}{\varepsilon_0} \sum_{r=\pm} \oint_{\gamma_p^r} \mathbf{f}_p^r \cdot \mathbf{t}_p^r P_{b,n}^{(2\omega)}|_{\gamma_{p,i}^r} dS \quad (\text{C18})$$

Combining in eq. C16 the derived expressions for the terms I_1 and I_2 we obtain:

$$\langle \mathbf{f}_p, \boldsymbol{\pi}_b^{(2\omega)} \rangle = \frac{1}{2\varepsilon_0} \sum_{r=\pm} \oint_{\gamma_p^r} (\mathbf{f}_p^r \cdot \mathbf{t}_p^r) \left[P_{b,n}^{(2\omega)}|_{\gamma_{p,e}^r} + P_{b,n}^{(2\omega)}|_{\gamma_{p,i}^r} \right] dl \quad (\text{C19})$$

-
- [1] Maier, *Plasmonics: Fundamental and Applications*. Springer, 2007.
- [2] A. Bouhelier, M. Beversluis, A. Hartschuh, and L. Novotny, "Near-field second-harmonic generation induced by local field enhancement," *Phys. Rev. Lett.*, vol. 90, p. 013903, Jan 2003.
- [3] T. F. Heinz, "Chapter 5," in *Nonlinear Surface Electromagnetic Phenomena* (H.-E. Ponath and G. I. Stegeman, eds.), pp. 397–405, North-Holland, Amsterdam, 1991.
- [4] J. I. Dadap, J. Shan, K. B. Eisenthal, and T. F. Heinz, "Second-harmonic rayleigh scattering from a sphere of centrosymmetric material," *Phys. Rev. Lett.*, vol. 83, pp. 4045–4048, Nov 1999.
- [5] P. Guyot-Sionnest, W. Chen, and Y. R. Shen, "General considerations on optical second-harmonic generation from surfaces and interfaces," *Phys. Rev. B*, vol. 33, pp. 8254–8263, Jun 1986.
- [6] W. L. Mochán, J. A. Maytorena, B. S. Mendoza, and V. L. Brudny, "Second-harmonic generation in arrays of spherical particles," *Phys. Rev. B*, vol. 68, p. 085318, Aug 2003.
- [7] J. I. Dadap, J. Shan, and T. F. Heinz, "Theory of optical second-harmonic generation from a sphere of centrosymmetric material: small-particle limit," *J. Opt. Soc. Am. B*, vol. 21, pp. 1328–1347, Jul 2004.
- [8] Y. Pavlyukh and W. Hübner, "Nonlinear mie scattering from spherical particles," *Phys. Rev. B*, vol. 70, p. 245434, Dec 2004.
- [9] J. Xu and X. Zhang, "Second harmonic generation in three-dimensional structures based on homogeneous centrosymmetric metallic spheres," *Opt. Express*, vol. 20, pp. 1668–1684, Jan 2012.
- [10] C. I. Valencia, E. R. Méndez, and B. S. Mendoza, "Second-harmonic generation in the scattering of light by an infinite cylinder," *J. Opt. Soc. Am. B*, vol. 21, pp. 36–44, Jan 2004.
- [11] C. Forestiere, G. Iadarola, G. Rubinacci, A. Tamburrino, L. D. Negro, and G. Miano, "Surface integral formulations for the design of plasmonic nanostructures," *J. Opt. Soc. Am. A*, vol. 29, pp. 2314–2327, Nov 2012.
- [12] A. G. F. de Beer, S. Roke, and J. I. Dadap, "Theory of optical second-harmonic and sum-frequency scattering from arbitrarily shaped particles," *J. Opt. Soc. Am. B*, vol. 28, pp. 1374–1384, Jun 2011.
- [13] J. Mäkitalo, S. Suuriniemi, and M. Kauranen, "Boundary element method for surface nonlinear optics of nanoparticles," *Opt. Express*, vol. 19, pp. 23386–23399, Nov 2011.
- [14] A. Benedetti, M. Centini, M. Bertolotti, and C. Sibilia, "Second harmonic generation from 3d nanoantennas: on the surface and bulk contributions by far-field pattern analysis," *Opt. Express*, vol. 19, pp. 26752–26767, Dec 2011.
- [15] A. Capretti, C. Forestiere, L. Dal Negro, and G. Miano, "Second harmonic generation in metal nano-spheres: a full-wave analytical solution with both local-surface and nonlocal-bulk non-linear sources," arXiv:1301.1628, 2013.
- [16] F. X. Wang, F. J. Rodriguez, W. M. Albers, R. Ahorinta, J. E. Sipe, and M. Kauranen, "Surface and bulk contributions to the second-order nonlinear optical response of a gold film," *Phys. Rev. B*, vol. 80, p. 233402, Dec 2009.
- [17] R. Harrington, *Field Computation by Moment Methods*. New York: Macmillan, 1968.
- [18] S. Rao, D. Wilton, and A. Glisson, "Electromagnetic scattering by surfaces of arbitrary shape," *Antennas and Propagation, IEEE Transactions on*, vol. 30, pp. 409–418, may 1982.
- [19] G. Bachelier, J. Butet, I. Russier-Antoine, C. Jonin,

- E. Benichou, and P.-F. Brevet, "Origin of optical second-harmonic generation in spherical gold nanoparticles: Local surface and nonlocal bulk contributions," *Phys. Rev. B*, vol. 82, p. 235403, Dec 2010.
- [20] J. Rudnick and E. A. Stern, "Second-harmonic radiation from metal surfaces," *Phys. Rev. B*, vol. 4, pp. 4274–4290, Dec 1971.
- [21] P. B. Johnson and R. W. Christy, "Optical constants of the noble metals," *Phys. Rev. B*, vol. 6, pp. 4370–4379, Dec 1972.
- [22] R. Graglia, "On the numerical integration of the linear shape functions times the 3-d green's function or its gradient on a plane triangle," *Antennas and Propagation, IEEE Transactions on*, vol. 41, pp. 1448–1455, oct 1993.
- [23] G. Gonella, W. Gan, B. Xu, and H.-L. Dai, "The effect of composition, morphology, and susceptibility on nonlinear light scattering from metallic and dielectric nanoparticles," *The Journal of Physical Chemistry Letters*, vol. 3, no. 19, pp. 2877–2881, 2012.
- [24] T. Hanke, G. Krauss, D. Träutlein, B. Wild, R. Bratschitsch, and A. Leitenstorfer, "Efficient nonlinear light emission of single gold optical antennas driven by few-cycle near-infrared pulses," *Phys. Rev. Lett.*, vol. 103, p. 257404, Dec 2009.
- [25] B. K. Canfield, H. Hsu, J. Laukkanen, B. Bai, M. Kuitinen, J. Turunen, and M. Kauranen, "Local field asymmetry drives second-harmonic generation in noncentrosymmetric nanodimers," *Nano Letters*, vol. 7, no. 5, pp. 1251–1255, 2007.